Level-Set Surface Segmentation and Fast Cortical Range Image Tracking for Computing Intrasurgical Deformations

M.A. Audette[1], K. Siddiqi[2], and T.M. Peters[3]

[1] Montreal Neurological Institute (McGill University), Montreal, Canada
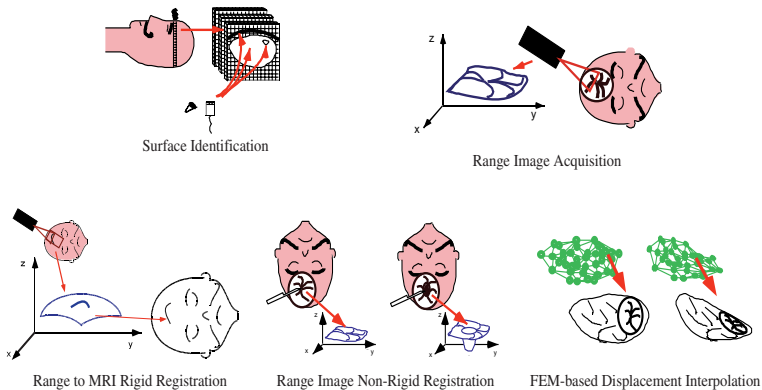maudette@nil.mni.mcgill.ca
[2] McGill Center for Intelligent Machines (McGill University), Montreal, Canada
siddiqi@cim.mcgill.ca
[3] The John P. Robarts Research Institute, London, Ontario, Canada
tpeters@irus.rri.on.ca

Abstract. We propose a method for estimating intrasurgical brain shift for image-guided surgery. This method consists of five stages: the identification of relevant anatomical surfaces within the MRI/CT volume, range-sensing of the skin and cortex in the OR, rigid registration of the skin range image with its MRI/CT homologue, non-rigid motion tracking over time of cortical range images, and lastly, interpolation of this surface displacement information over the whole brain volume via a realistically valued finite element model of the head. This papers focuses on the anatomical surface identification and cortical range surface tracking problems. The surface identification scheme implements a recent algorithm which imbeds 3D surface segmentation as the level-set of a 4D moving front. A by-product of this stage is a Euclidean distance and closest point map which is later exploited to speed up the rigid and non-rigid surface registration. The range-sensor uses both laser-based triangulation and defocusing techniques to produce a 2D range profile, and is linearly swept across the skin or cortical surface to produce a 3D range image. The surface registration technique is of the iterative closest point type, where each iteration benefits from looking up, rather than searching for, explicit closest point pairs. These explicit point pairs in turn are used in conjunction with a closed-form SVD-based rigid transformation computation and with fast recursive splines to make each rigid and non-rigid registration iteration essentially instantaneous. Our method is validated with a novel deformable brain-shaped phantom, made of Polyvinyl Alcohol Cryogel.

1 Introduction

Image-guided surgery is a technique whereby a model of a patient's head, typically featuring skin, cortex and lesion surfaces, is constructed from a set of segmented MRI/CT images and is then registered with the patient's head in the OR, using a locating device. The usefulness of this technology hinges on the

Fig. 1. Brain shift estimation framework

accuracy of the transformation between the image and patient spaces. However, this transformation becomes less accurate as the brain shifts during surgery.

To alleviate this problem, we propose a method for estimating brain shift which is characterized by the following stages (see figure 1):

- semi-automatic identification (segmentation) of relevant anatomical surfaces within the MRI/CT volume;
- range-sensing of the skin and cortex in the OR;
- rigid registration of the skin range image with its MRI/CT homologue, which will serve as a baseline for the next stage;
- non-rigid motion tracking, over time, of the cortical range image;
- and lastly, interpolation of the resulting surface displacement over the whole brain volume, assuming null displacement at the base of the skull, via a realistic finite element model (FEM).

Our discussion here focuses on identification of anatomical surfaces by level-set segmentation, range-sensing of visible anatomical surfaces, and cortical motion estimation. We also describe a novel phantom design, whose material properties and shape are very good approximations of those of the human brain. This phantom will be used to validate our research on intrasurgical motion estimation.

Intrasurgical brain shift has been documented by Maurer [13] and by Skrinjar [19], who attribute it to the effect of gravity, to a gradual seepage of CSF, to cerebral blood volume manipulation, and to the effect of certain drugs. Existing techniques for dealing with brain shift include intraoperative MR scanners [13] and intraoperative ultrasound [7]. Miga [14] and Škrinjar [19] have independently developed FEM-based solutions in the same spirit as ours, although we emphasize the estimation of a dense surface displacement function, which is then interpolated over the brain volume (assuming null displacement at the base of the head), whereas their work focuses on the physical modelling which most realistically performs this interpolation or generically models this phenomenon.

Our goal is to first demonstrate the proof of concept of a technique integrating surface displacement estimation and finite-element modelling, with a highly accurate range-sensor and a brain-shaped phantom made of a well-characterized elastic material. A method based on surface displacement estimation and finite-element modelling is extremely compelling from a strictly economic standpoint, as the combination of range-sensor and FEM software is significantly cheaper than ultrasound or intraoperative MR. Moreover, our method also benefits from the speed, ease-of-use, and accuracy of range-sensors and state-of-the-art physical models. Also, our method does not preclude the integration of resection information, provided by a tracked hand-held probe [17] for example. Lastly, a surface displacement-FEM framework, minus the range-sensor, constitutes the foundation of a realistic patient-specific *surgical simulation* system, at the cost of a haptic feedback device, some optimization of the FEM computation for this environment, and modelling of surgical tools.

This paper is organized as follows. After the introduction, a presentation of our materials and methods is given in § 2, namely level-set segmentation of the skin and cortex (§ 2.1), range-sensing of the same two surfaces in the OR (§ 2.2), cortical motion estimation (§ 2.3), and an elastic brain phantom (§ 2.4). The results appear in § 3, and we discuss the results and future directions in § 4.

2   Materials and Methods
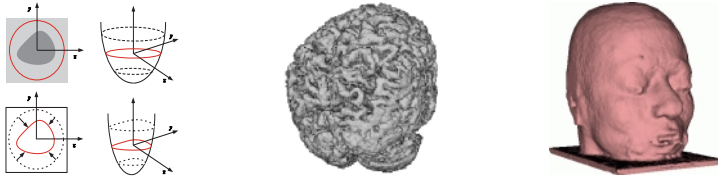
2.1   Level-Set Surface Segmentation

The skin and cortex surface identification technique is an implementation of a recent algorithm, known as a *surface evolution* model, which imbeds 3D surface segmentation as the zero level-set of a 4D hypersurface Ψ, as illustrated in figure 2(a) for the problem of lesser dimensionality, namely identifying 2D contours. This approach possesses certain advantages over physically-based models, in particular its capacity to capture a large variety of topologies and a relative insensitivity to initial conditions [12].

In general, a surface evolution model is initialized by a user-defined surface completely inside (or outside) the desired anatomical boundary. The front then moves in a strictly outward (inward) manner as the zero level set of the evolving hypersuface [23]:

$$\frac{\partial \Psi}{\partial t} \;=\; \phi(x,y,z)\|\nabla\Psi\|(H+\nu) \;+\; \nabla\phi \cdot \nabla\Psi \;, \tag{1}$$

where mean curvature H of the front is given by $div(\nabla\Psi/\|\nabla\Psi\|)$.

The model features a diffusive term $\|\nabla\Psi\|H$ which tends to smooth out the front, a hyperbolic term $\|\nabla\Psi\|\nu$ which pushes the front forward while preserving discontinuities, and two image terms: a speed function ϕ which slows down the front near strong gradients, and a so-called "doublet" term $\nabla\phi \cdot \nabla\Psi$ which prevents the front from overshooting these gradients. This model has been further

Fig. 2. Level-set segmentation: (a) imbedding of 2D contour estimation in 3D; (b) 3D surface of the cortex (seen from behind the occipital lobe), obtained with an outward-moving front initialized with 18 small spheres in the white matter (c) 3D surface of the skin, identified with an inward-moving front initialized at the scan perimeter.

generalized in [18]. The image cofactor ϕ is expressed as

$$\phi \; = \; \frac{1}{1 + \|\nabla \tilde{I}(x,y,z)\|^n} \; , \tag{2}$$

where $\tilde{I}(x,y,z)$ is the *anisotropically* filtered equivalent of the original volume $I(x,y,z)$ and $n = 2$ or 3. We filter anisotropically, prior to computing gradients, because we will eventually *register* the result of the segmentation operation with a skin or cortex range image, and want to prevent unwanted blurring across relevant anatomical surfaces. This preprocessing is actually implemented within a level-set framework, namely by inputing the raw MRI/CT volume (as opposed to a distance map defined over the same volume) to a surface evolution model, but with only the diffusive term computation enabled [8]. Moreover, anatomical information can be taken into account by considering the result of an *Artificial Neural Network* (ANN) voxel classifier [10], in defining the image cofactor, for example to prevent an outward front from getting snagged at the grey matter-white matter boundary. Also, to reduce the complexity of computing a 4D, rather than 3D, function, we adopt the *narrow band* approach proposed by Adelsteinsson [1], which restricts the computation of the evolution equation near the evolving 3D surface.

A distance map is computed from the final surface by the fast marching level-set method [16], which estimates the arrival time $T(x,y,z)$ of a monotically advancing front by expressing an evolution equation of the type $\Psi_t + \phi(x,y,z)\|\nabla\Psi\| = 0$ as the Eikonal relation $\|\nabla T\|\phi = 1$. By using a constant unit speed ($\phi = 1$), this arrival time function corresponds to a *sub-pixel Euclidean distance map* [9]. Moreover, the propagative nature of the algorithm can be exploited to reveal *which surface point is closest to a given voxel* (i.e.: which surface point possesses the shortest arrival time). The relevance of this map is emphasized in § 2.3.

Lastly, not only is this segmentation technique useful in identifying the cortex and skin for the purpose of registration, we can further exploit it to label the nodes of our patient-specific finite-element model, according to tissue type, by combining the nodes initially circumscribed by the analytical user-defined surface

with those traversed by the moving front. With this application in mind, we can also segment the external surface of tumours and ventricles.

2.2   Range-Sensing

The three-dimensional coordinates of the visible surfaces of the skin and evolving cortex are computed by a commercial range-sensor made by Vitana Corp. (Ottawa, Canada), which uses both laser-based *triangulation* and *defocusing* techniques to estimate range [22]. Laser-based range-sensing is the industrial standard for quickly and accurately acquiring dense, quantitative information on 3D shape, used for example in robotic navigation, industrial quality control, and welding automation.

Triangulation involves projecting a thin ray of laser light onto an object, capturing the reflected light by a charge-coupled device (CCD), and inferring depth from the trigonometric relationship relating the pixel position of the reflected point, the position of the laser source and the CCD. Defocusing is implemented by allowing the laser light to pass through a mask featuring *two* holes, at a predetermined distance d apart, rather than one. The CCD sees two laser profiles instead of one, and range is determined by measuring the space (in each pixel column) between the two images. The sensor has .5mm pixel accuracy, based on a depth of field of 135mm and field of view of 10-12cm. During its linear travel, our program acquires 256 laser profiles at a constant rate, when the positioner is known to move at a constant speed. The *equal spacing* of our samples, resulting from the CCD being regular (in the i-k pixel coordinates, not in x-z spatial coordinates) and from constant-rate acquisition along the y-axis, is exploited later on in the registration process.

2.3   Surface Displacement Estimation

We estimate cortical surface deformation by first establishing a baseline for this movement, then by registering the initial cortical range image with its homologue identified in the MRI volume, and finally by tracking non-rigid cortical surface motion between time t_n and time t_{n+1}. Currently, we work with a brain-shaped phantom which does not possess a skin or a bone layer, and obtain this movement baseline by manually providing a rough alignment (based on the four corners of the range image domain) between the initial range and MRI surfaces of this phantom, and by refining it with a rigid-body registration to initial range data. The rigid-body refinement, at t_0, and all subsequent non-rigid stages of cortical registration are implemented with an *iterative closest point* (ICP) technique [5,11]. This technique provides a much denser displacement map than a feature-based technique, which is important to best quantify non-rigid surface motion, which in turn is fundamentally underdetermined.

Our iterative registration technique bears some comparison to that of Lavallée and Szeliski [11], in that a distance map is precomputed for the MRI volume from the identified cortical surface, thereby accelerating the computation of distances between closest-point pairs, rather than imposing an expensive search

for them. Because the Lavallée method produces only distances between closest point pairs, but does not provide information about which particular point is closest, it must resort to a search method, such as Levenberg-Marquardt, to determine the optimal transformation. In contrast, closed-form methods for computing transformation parameters all require *explicit* point-pairs, not distances between them. As emphasized in § 2.1, we make use of the fast marching level-set method to produce a dense map of both *closest point labels and the distances to them*, allowing us to do away with a search for closest points as well as producing explicit point pairs which can take advantage of closed-form transformation algorithms, thereby making each iteration of our ICP technique essentially instantaneous. We currently use Arun's SVD [3] technique to compute the rigid transformation between the two sets of points.

The non-rigid registration stage uses the same ICP matching technique to produce a smoothed displacement vector function. The expression of the deformation over a 2D domain is a consequence of our explicit displacement information being available only on an open surface, below and outside of which we defer to a realistically valued finite-element model to estimate volumetric movement. Furthermore, in characterizing non-rigid surface movement, we can exploit the regularity of the range domain by using Unser's extremely efficient *recursive splines* [21]. The justification for emphasizing computational efficiency here is two-pronged: *clinical acceptability* and the inherent *temporal underdetermination* in estimating non-rigid motion. We adopt a *smoothing spline* approach, whose first stage is a convolution with a smoothing kernel [1]

$$S_\lambda^n(Z) \;=\; 1/\left(B_1^n(Z) + \lambda(-Z + 2 - Z^{-1})^{\frac{n+1}{2}} \right) , \tag{3}$$

where $B_1^n(Z)$ is the *indirect B-spline transform* given by Unser [21], n is the order of the spline fitting (we use a linear fit: $n = 1$) and λ is the regularization parameter of the smoothing. This stage produces B-spline coefficients and is followed by a convolution with the indirect transform $B_1^n(Z)$ to yield the smoothed output. The filters can simply be cascaded to implement smoothing in 2D. In order to make the non-rigid motion estimation well-behaved, the smoothing parameter λ is initially set very high, and is gradually lowered as the process iterates, progressively resolving finer-level motion detail. Just as for the rigid ICP stage, each iteration of the non-rigid surface motion estimation is essentially instantaneous.

2.4   Elastic Brain Phantom

For the purpose of reproducing non-rigid cortical movement, we have implemented a brain-shaped phantom with elastic material properties. We use a jello mold in the shape of the brain (obtained from the Anatomical Products Online website [2]), into which we pour *PolyVinyl Alcohol Cryogel* (PVA-C), as illustrated in figure 3(a). The latter is a relatively *viscous liquid*, which upon freezing

---

[1] Note: Z here relates to the Z-transform, not to be confused with the depth axis of the range-sensor.

Fig. 3. Elastic PVA-C brain phantom: (a) liquid stage (b) final result after freezing and thawing.
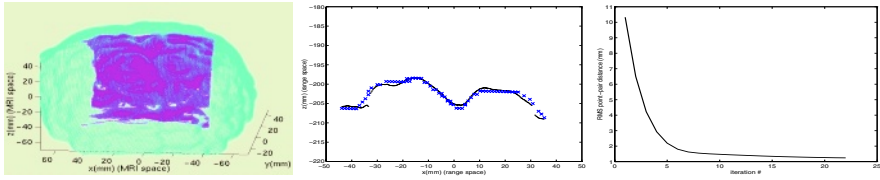
and thawing, becomes an *elastic solid* [6] as shown in figure 3(b). Furthermore, PVA-C can sustain several freeze-thaw cycles to acquire more rigidity, and the PVA concentration can also be manipulated to that effect, producing a Young's modulus E in the .1 to .7 MPa spectrum [20]. This is comparable to values published in the literature for gray and white matter material properties [24]. This phantom features a moving assembly consisting of a small disk and rod of plexiglass, imbedded within the elastic material, as well as some glass beads used to validate the surface displacement/FEM approach to volumetric motion estimation. The position of the moving assembly can be modified by means of some set screws, drawing the embedded disk toward its support plate and triggering a compression of the elastic material.

3   Results and Discussion

Our segmentation implementation produces the expected results, as apparent in figure 2. The only new finding we report is the consideration of voxel classification results in making the image cofactor account for prior anatomical information. One of the main contributions of this paper, namely that the level-set framework leads to a very efficient iterative surface registration, is simply a fortuitous by-product of our segmentation design choice.

Our tests indicate that our implementation of an iterative closest point registration efficiently produces results comparable to other ICP techniques, as shown in figures 4 and 5 for rigid and non-rigid registration respectively. The algorithm, given a good starting point, does indeed converge to a very good pose estimation. The results of figure 4 are based on an initial alignment carried out by choosing four points on the level-set surface which roughly correspond to the corners of the range image, to which an arbitrary vertical distance of 15 pixels, or roughly 13.5mm was added.

In order to assess non-rigid surface tracking, we turn the set screws under the support plate of our elastic phantom, triggering a deformation of up to 15mm at the top, and image the cortical surface with our range-sensor, while maintaining the support plate fixed with respect to the range-sensor/positioner reference (see figure 3(b)). We then compare the results of a strictly rigid transformation computation with a sequence of rigid and non-rigid ICP registrations. Each option uses the same rough initial alignment based on the corners of the range
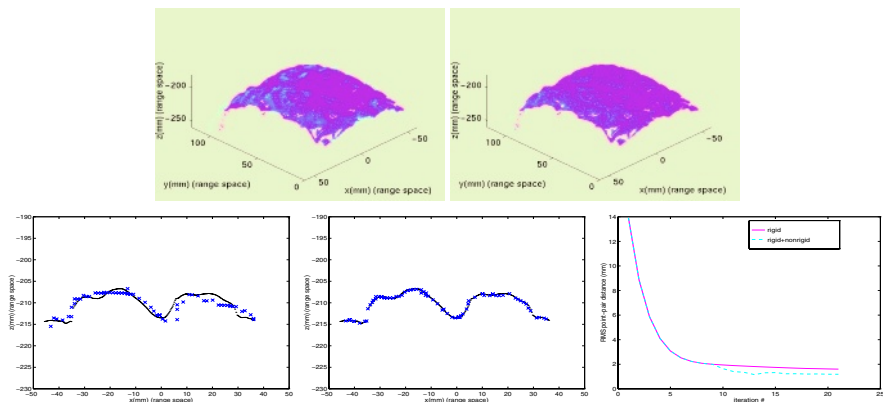
Fig. 4. Typical rigid registration results: (a) transformed range image overlaid on MRI level-set surface (both decimated by a factor of 2 for readability), in MRI space; (b) single range profile ($j = 192$ or $y = 79.592$) with projections of closest MRI points on $y = 79.592$ plane, in range space; (c) RMS point-pair distance plotted against ICP iteration number.

domain. This comparison is currently based on visual inspection of how the original MRI level-set surface, subject to the inverse of the range-to-MRI transformation, aligns with the range data of the deformed cortical surface, and on the two plots of the RMS distance between point-pairs against iteration number. The abrupt improvement of RMS distance on the second curve indicates the onset of the non-rigid stage, with an earlier rigid stage termination than the rigid-body stage illustrated by the first curve.

The RMS point-pair distance which appears in figures 4 may in fact overestimate the registration error between the two surfaces, due to the range data being much denser than the overlapping MRI-voxels which constitute the homologous patch of the level-set surface (65536 vs. 5782 points). In other words, because the ICP range-to-level set matches can be *many-to-one*, the point-pair distance has a large component which lies in the plane normal to the vector along the shortest path between the two surfaces which emanates from each level-set surface voxel. Furthermore, if the displacement vectors between the original (many-to-one) closest point pairs are used to determine the non-rigid spline-based transformation, we find that they distort the displacement map by inflating the components normal to the shortest path at each point between the two surfaces. We obtain better results by considering only the displacements of *mutually* closest (i.e.: one-to-one) pairs, which can be determined fairly easily from the original set of point pairs, and by iteratively propagating this displacement information everywhere else (this appears in figure 5).

Future registration work includes a *calibration* procedure which will relate points in range-sensor space to points in a global coordinate system in the OR, in a manner similar to Comeau's technique for relating the position of ultrasound data to a global OR reference [7]. This will serve as a good initial alignment for our rigid-body ICP range-MRI skin registration stage. Further work will address the sensitivity of ICP-type methods to initial alignment [5]. Finally, a validation of the surface tracking/FEM framework, by tracking glass beads imbedded in the brain phantom, is also planned.

Fig. 5. Typical non-rigid registration results: (a) MRI level-set surface rigidly registered to the range image of the deformed phantom, in range space (both decimated by a factor of 2); (b) MRI level-set surface non-rigidly registered to the range image of the deformed phantom (both decimated by a factor of 2); (c) slice through (a), at $y = 79.592$; (d) slice through (b), at $y = 79.592$; (e) evolution of RMS point-pair distance with ICP iteration.

4   Conclusion

This paper proposes a novel means of estimating intrasurgical deformations, based on level-set segmentation, range-sensing of the skin and cortex, fast rigid and non-rigid surface registration, and finite-element based estimation of volumetric displacement. We have emphasized some of the machine vision issues in this approach, in particular how the level-set framework can be exploited to yield computational speedups in the surface registration. The use of recursive splines is also a factor in our algorithmic efficiency. We have also presented a new brain-shaped elastic phantom with which non-rigid cortical movement can be enacted and our method can be validated.

Acknowledgements

References

1. D. Adelsteinsson & J.A. Sethian, A Fast Level Set Method for Propagating Interfaces, *J. Computational Physics*, No. 118, pp. 269-277, 1995. 791
2. Anatomical Products Online: *www.anatomical.com/catalogs/product/21013brainmold.html*, 1998. 793
3. K.S. Arun et al., Least-squares Fitting of Two 3-D Point Sets, *IEEE Trans. Pattern Analysis & Machine Intelligence*, Vol. 9, No. 5, pp. 698-700, May 1987. 793
4. M.A. Audette, F.P. Ferrie & T.M. Peters, An Algorithmic Overview of Surface Registration Techniques for Medical Imaging, *Medical Image Analysis*, submitted.
5. P.J. Besl & N.D. McKay, A Method for Registration of 3-D Shapes, *IEEE Trans. Pattern Analysis & Machine Intelligence*, Vol.14, No.2, pp. 239-256, 1992. 792, 795
6. K.C. Chu & B.K. Rutt, Polyvinyl Alcohol Cryogel: An Ideal Phantom Material for MR Studies of Arterial Flow and Elasticity, *Magnetic Resonance in Medicine*, No. 37, pp. 314-319, 1997. 794
7. R.M. Comeau, A.F. Sadikot, A. Fenster & T.M. Peters, Intraoperative Ultrasound for Guidance and Tissue Shift Correction in Image-guided Neurosurgery, *Medical Physics*, submitted, 1999. 789, 795
8. B.B. Kimia & K. Siddiqi, Geometric Heat Equation and Nonlinear Diffusion of Shapes and Images, *Computer Vision and Image Understanding*, Vol. 64, No. 3, pp. 305-322, Nov. 1996. 791
9. R. Kimmel, N. Kiryati, and A.M. Bruckstein. Sub-pixel Distance Maps and Weighted Distance Transforms, *J. Mathematical Imaging and Vision*, No. 6, pp. 223-233, 1996. 791
10. V. Kollokian, *Performance Analysis of Automatic Techniques for Tissue Classification in MRI of the Human Brain*, Master's thesis, Concordia University, Montreal, Canada, November 1996. 791
11. S. Lavallée & R. Szeliski, Recovering the Position and Orientation of Free-form Objects from Image Contours Using 3D Distance Maps, *IEEE Trans. Pattern Analysis & Machine Intelligence*, Vol. 17, no. 4, pp. 378-390, 1995. 792
12. R. Malladi, J.A. Sethian & B.C Vemuri, Shape Modeling with Front Propagation: A Level Set Approach, *IEEE Trans. Pattern Analysis & Machine Intelligence*, Vol. 17, No. 2, Feb. 1995. 790
13. C.R. Maurer et al., Measurement of Intraoperative Brain Deformation Using a 1.5 Tesla Interventional MR System: Preliminary Results, *IEEE Trans. Medical Imaging*, Vol. 17, No. 5, pp. 817-825, Oct. 1998. 789
14. M. I. Miga et al., A 3D Brain Deformation Model Experiencing Comparable Surgical Loads, Proc. 19th Int. Conf. IEEE EMBS, pp. 773-776, 1997. 789
15. H. Murase & S.K. Nayar, Visual Learning and Recognition of 3-D Objects from Appearance, *Int. J. Computer Vision*, No. 14, pp. 5-24, 1995.
16. J.A. Sethian, Fast Marching Level Set Method for Monotonically Advancing Fronts, *Proc. Nat. Acad. Sci. USA*, Vol. 93, pp. 1591-1595, Feb. 1996. 791
17. M. Sinasac & T.M. Peters, Use of 3-D Deformable Surface Models for Intraoperative Visualization and Quantification of Cerebral Tissue Resection, *Medical Physics*, Vol. 24, No. 7, p. 1211, July 1997. 790
18. Kaleem Siddiqi et al., Area and Length-Minimizing Flows for Shape Segmentation, *IEEE Transactions on Image Processing*, Vol. 7, No. 3, pp. 433-443, 1998. 791
19. O. Škrinjar, D. Spencer & J. Duncan, Brain Shift Modeling for Use in Neurosurgery, *Medical Image Computing and Computer-Assisted Intervention- MICCAI'98*, pp. 641-649, 1998. 789

20. K. Surry, *www.irus.rri.on.ca/∼kath*, 1999.   794
21. M. Unser, A. Aldroubi, & M. Eden, B-Spline Signal Processing: Part I- Theory, *IEEE Trans. Signal Proc.*, Vol. 41, No. 2, pp 821-833, Feb. 1993.   793
22. Vitana Corporation, *ShapeGrabber Reference Manual*, 1997.   792
23. A. Yezzi Jr. et al., A Geometric Snake Model for Segmentation of Medical Imagery, *IEEE Trans. Medical Imaging*, Vol. 16, No. 2, pp. 199-209, Apr. 1997.   790
24. C. Zhou, T.B. Khalil, & A.I. King, A New Model Comparing Impact Responses of the Homogeneous and Inhomogeneous Human Brain, *Society of Automotive Engineers, Inc. report #952714*, 1995.   794